ON THE CONTROL OF A 155 MM SPIN-STABILIZED PROJECTILE USING THE COANDA EFFECT

Mickael Zeidler[1], Eric Garnier[2], Roxan Cayzac[1] and Alain Merlen[2]
[1]*NEXTER Munitions, 7 route de Guerry - F-18023, Bourges, France*
[2]*ONERA-The French Aerospace Lab, 8 rue des Vertugadins-F-92190, Meudon, France*

This paper aims at investigating numerically the control of a 155 mm spin-stabilized projectile using the Coanda effect. A tangentially blowing jet exits over a convex surface at the projectile base and generates significant aerodynamic efforts. In the first part, RANS simulations are performed without projectile rotation. Numerous continuous blowing conditions are assessed. The variation of the normal force coefficient with respect to the momentum coefficient is presented for four free stream Mach numbers. In the second part, URANS simulations with a 400 Hz rotation are performed. A pulsed jet is used in phase with the rotation to act in a 90° sector centered in the lift plane, leading to a non-zero normal force increment. Then, four pulsed jets equally distributed along the projectile circumference are simulated to further improve the control authority. The jet separation process is investigated to determine the azimuthal influence of the jet on the control.

INTRODUCTION

In order to both reduce collateral damages and improve the lethality of weapon systems, manufacturers are increasingly studying projectiles incorporating a trajectory correction capability. The main issue for ballistic research engineers is to be able to generate downrange or cross-range efforts to ensure a trajectory correction larger than the standard deviation of the projectile. Mechanical actuators like fins, spoilers, or canards have already proved their efficiency for aero-stabilized projectiles (see [1] and [2]). Many studies have also been pursued from the last sixty years on the control of aero-stabilized projectiles using fluidic actuators (see [3] and [4]). But, despite the large number of studies concerning aero-stabilized projectiles, a few have been developed for spin-stabilized ones. The wide flight domain and the high spin rate of the projectile complicate particularly its guidance. Consequently, control devices have to be actuated at the projectile spin rate to permit a significant deviation. McMichael et al. [5] proposed to steer a 44 mm subsonic spinning munition using the Coanda effect. Four piezoelectric synthetic jets acting at a frequency of f=1 kHz blow over a convex surface and induce localized flow attachment. This investigation is incorporated within the framework of the DARPA's project "Scorpion" to design a guided subsonic munition and several studies have been published on this prototype ([5], [6], [7] and [8]). Nevertheless, those works have been realized for low free stream velocities applications. In practice, the flight domain of a large-caliber projectile ranges from M_∞=0.7 to M_∞=3.0. The goal of this study is also to investigate if the Coanda effect can be used for such Mach numbers and for a large-caliber projectile.

NUMERICAL CONFIGURATION

Computational Mesh

The geometry used in the present study is a 155 mm high explosive (HE) model. This particular configuration is chosen because measurements of global coefficients led by Nexter Munitions are available on a wide range of free stream conditions, allowing validation of simulations. Two block-structured meshes are generated for subsonic and supersonic free stream conditions, encompassing respectively 5.8 and 4.6 millions points for the baseline configuration (see figure 1(a)).

Geometrical modifications are achieved at the aft end of the projectile to design the Coanda convex surface (see figure 1(b)). A jet extends 18° azimuthally and emanates from a backward-facing step over a circular surface which radius is such that R_c/R=33%, R denoting the projectile radius. The height h_c of this step is thin enough to enable local flow attachment with actuation and high enough to prevent attachment without actuation. The height of the jet scales with half the height of the step (h_c/R=3% and h_j/R=1.5%). These values are chosen identical to those of McMichael et al. work [5]. Meshes are refined along the Coanda surface to capture the streamwise evolution of the boundary layer and encompass 9.6 millions points for subsonic free stream conditions and 8.3 millions for supersonic ones.

The els*A* Solver

The CFD solver used in this study is the Onera's software els*A*, which is based on a cell centered finite volume approach to solve the Navier-Stokes equations on a structured multi-block grid. A classical Roe scheme is used with a "minmod" limiter and a Harten's coefficient set to 0.1. The turbulence model of Spalart and Allmaras is retained. RANS and URANS simulations are performed for respectively the non-spinning and the spinning configuration. For steady simulations, a first-order accurate implicit scheme is used. For unsteady simulations, the solution is advanced in time using a "Gear" method. At convergence of this iterative process, the time advancement is second order accurate. Six sub-iterations using a Newton algorithm are performed. The grid is moved to take into account the rotation of the projectile.

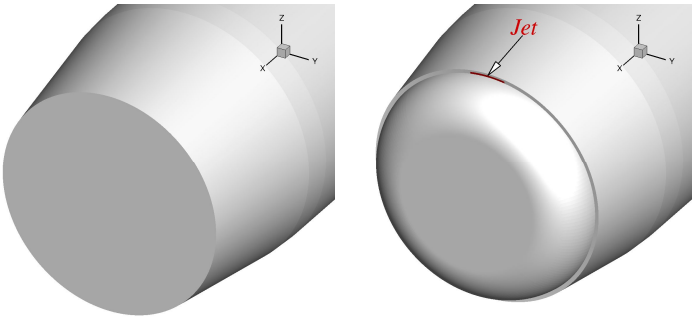

(a) Baseline configuration (b) Coanda-controlled configuration

Figure 1. Modification of the projectile aft end. The red area shows the localization of the jet.

RESULTS VALIDATION OF THE BASELINE PROJECTILE

Non-Spinning Baseline Configuration

This section underlines the capacity of els*A* on this particular application by a comparison with two series of experiments conducted by Nexter Munitions for both the non-spinning and the spinning projectiles. Steady simulations are first compared with the available global aerodynamic coefficients for a non-spinning case. Four free stream Mach numbers (M_∞=0.7, 0.9, 1.2 and 2:0) are investigated for angles of attack varying from α=-2° to 18°. Comparisons between els*A* simulations and experiments are presented in figure 2 for M_∞=0.7 and M_∞=2.0. Note that the axial force coefficient C_A is obtained without taking into account the base pressure. In experiments, four sensors are used at the base of the projectile to evaluate a space averaged base pressure which is subtracted from the global axial force coefficient.

Numerical results are in close agreement with the experimental data for both the normal force coefficient C_N and the pitch coefficient C_m up to 10°. Even at higher angles of attack, differences between computations and experiments remain within the experimental uncertainties for every Mach number. Some discrepancies appear on the axial force coefficient C_A, especially at M_∞=0.7. This can be explained by the fact that most turbulence models fail to predict the massively separated flow behind the base. The error on the base pressure prediction can affect the pressure distribution upstream of the projectile aft end, explaining observed discrepancies for subsonic Mach number. Furthermore, the wind tunnel model is held with an aft sting, which can affect the evaluation of the base pressure.

Spinning Baseline Configuration

As for simulations of the non-spinning projectile, comparisons between Nexter Munitions experiments and els*A* computations are performed. The spin rate of the projectile is set to 400 Hz. Computations are only conducted at M_∞=0.9 and at M_∞=2.0 for an angle of attack of α=3°.

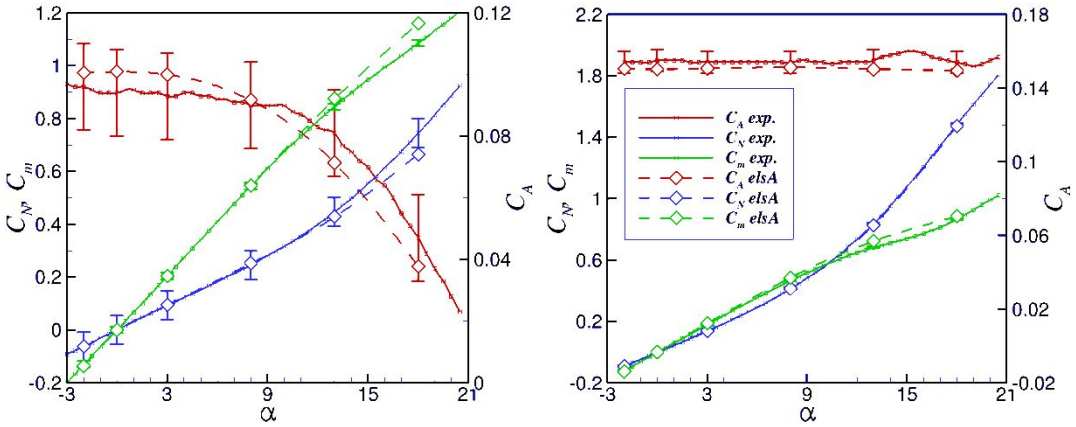

Figure 2. Comparisons between experiments and els*A* simulations. Experimental margins of error are displayed for computed angles.

TABLE I. ELS*A* SIMULATIONS AND NEXTER EXPERIMENTS COMPARISON AT M_∞=0.9 AND α=3° FOR THE SPIN-STABILIZED PROJECTILE.

Configuration	C_Y	C_N	C_m	C_n
Experiments	0.0169±24%	0.0902±4%	0.0264±1%	0.0136±22%
els*A* (7200 ite./rev)	0.0147	0.0921	0.02324	0.0102
Discrepancy els*A*/exp. (%)	+13%	+2%	-11%	-25%

TABLE II. ELS*A* SIMULATIONS AND NEXTER EXPERIMENTS COMPARISON AT M_∞=2.0 AND α=3° FOR THE SPIN-STABILIZED PROJECTILE.

Configuration	C_Y	C_N	C_m	C_n
Experiments	0.0075±40%	0.1412±2%	0.1849±1%	0.0056±0%
els*A* (7200 ite./rev)	0.0073	0.1397	0.1872	0.0056
Discrepancy els*A*/exp. (%)	-2%	-1%	+1%	0%

As shown in table I, a 11% discrepancy can be observed for the pitching moment coefficient C_m at M_∞=0.9, although the experimental uncertainty is only 1%. Note that the lateral effort is very weak and is affected by measurement uncertainties. Concerning supersonic flow, numerical results are in agreement with experiments and remain within the experimental margin of uncertainty (see table 2).

COANDA-CONTROLLED CONFIGURATION

Use of Continuous Blowing for the Non-Spinning Projectile

Computations are performed for the Coanda-controlled configuration at M_∞=0.7, 0.9, 1.2, and 2.0. The rotation of the projectile is not taken into account and two angles of attack α=0° and 3° are considered. Several blowing conditions are carried out using a boundary condition applied in the red area shown in figure 1(b).

GLOBAL RESULTS

The principal interest of this work is the study of the normal force increment for several momentum coefficients C_μ at subsonic, transonic, and supersonic free stream Mach numbers. Poisson-Quinton et al. [9] highlighted the fact that this momentum coefficient is the appropriate scaling parameter which allows to superimpose lift increment obtained with different slot widths. It is defined as:

$$C_\mu = \frac{\rho_j U_j^{\,2} S_j}{0.5 \rho_\infty U_\infty^{\,2} S_{ref}} \tag{1}$$

In our case, the jet density ρ_j and the jet velocity U_j are evaluated at the center of the jet slot. The reference surface S_{ref} is defined as $S_{ref}=\pi D^2/4$. Evolutions of ΔC_N for the four free stream Mach numbers are presented in figure 3, point labels indicating the jet Mach number. The normal force increment at M_∞=2.0 is almost zero (see figure 3(d)). No particular evolution with the steady momentum coefficient can be noticed and ΔC_N is both positive and negative for low values of C_μ (see zoom). At M_∞=1.2, the normal force increment is more important than at M_∞=2.0 and a linear evolution can be inferred for values of the momentum coefficient ranging from $C_\mu=5\times10^{-4}$ to 4×10^{-3}. Nevertheless, ΔC_N remains negligible.

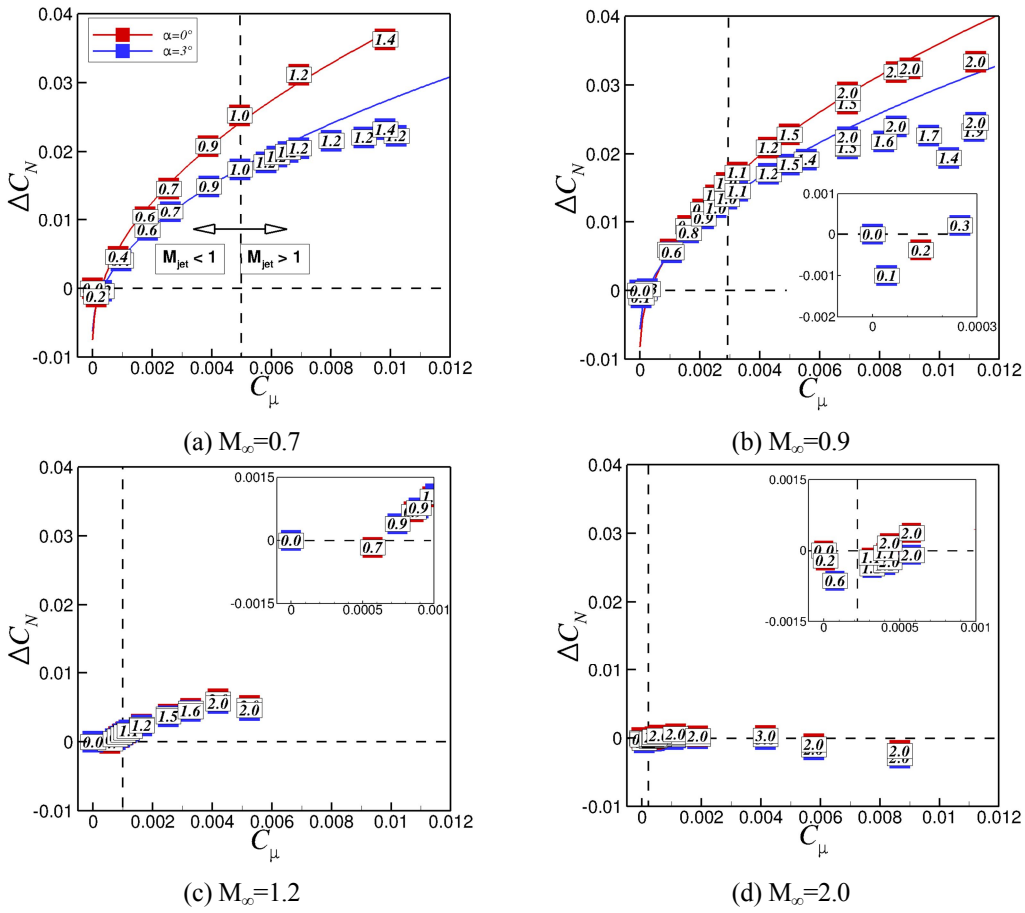

(a) M_∞=0.7 (b) M_∞=0.9

(c) M_∞=1.2 (d) M_∞=2.0

Figure 3. Evolution of ΔC_N with the momentum coefficient C_μ for the four free stream Mach numbers. Labels indicate jet Mach numbers and results (squared symbols) in figure (a) and (b) are interpolated using a square root function (curves).

Real benefits exist at M_∞=0.7 and at M_∞=0.9, where ΔC_N can reach 0.03 for high values of the momentum coefficient. This is equivalent to a variation of the angle of attack of 1°. According to Poisson-Quinton et al. [9], two evolutions of ΔC_N with C_μ can be obtained. At low values of the momentum coefficient, the normal force increment is proportional to C_μ and the control acts on the boundary layer to generate a flow that could be described by potential flow solutions. For higher values of C_μ, the evolution of the normal force increment is lower (ΔC_N is proportional to $\sqrt{C_\mu}$) and control acts on the circulation. Curves drawn in figures 3(a) and 3(b) interpolate results with a square root function. As shown here, the evolution of the normal force increment fits with a $\sqrt{C_\mu}$ evolution even at low values of C_μ which indicates a circulation control for the two subsonic free stream Mach numbers. Note that some efficiency loss appears with supersonic jet conditions, where ΔC_N increases at a lower rate than $\sqrt{C_\mu}$.

COANDA EFFECT WITH EXTERNAL SUPERSONIC FLOWS

As it was already highlighted in figure 3(c) and 3(d), ΔC_N is negligible at M_∞=1.2 and 2.0. The visualization of Mach number iso-contours in figure 4 allows to compare the Coanda jet behavior between transonic and supersonic regimes.

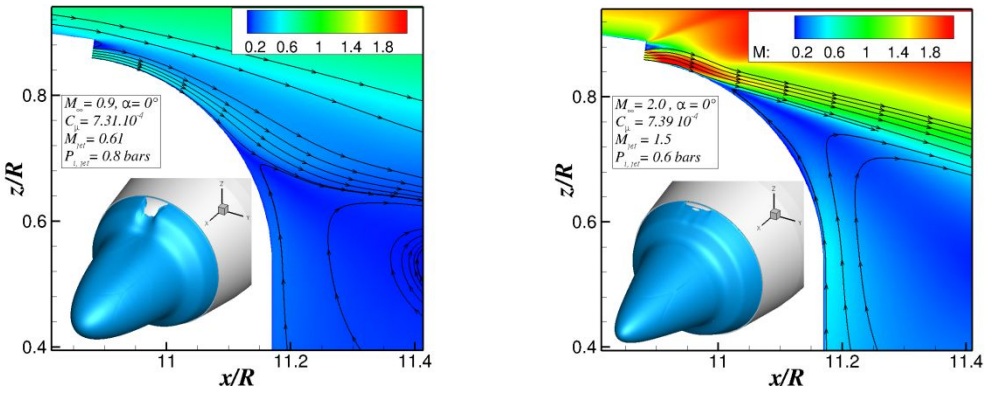

(a) M_∞=0.9 (b) M_∞=2.0

Figure 4. Iso-contours of Mach numbers in the xOz plane (main figures) and iso-surfaces of u=0 (bottom left).

Added iso-surfaces of zero longitudinal velocity make appear the Coanda wall surface where the jet is attached. At M_∞=2.0, the Coanda jet detaches near the slot and the surface where the jet is attached is limited. For every tested blowing condition at M_∞=2.0, the jet separation angle never exceeds 30°. At M_∞=0.9, the wall jet is really deviated by the convex surface and the attached surface is more important. The jet separation angle exceeds 50° for every blowing condition and a significant flow asymmetry induces aerodynamic efforts.

Streamwise integration of the normal force coefficient at α=0° and for the four computed Mach numbers is displayed in figure 5. Values of the momentum coefficient are almost identical for every computation. For supersonic free stream Mach numbers, control acts only downstream from the slot. There is no circulation control because supersonic flow prohibits the propagation of upstream pressure waves. Moreover, at M_∞=2.0, the jet creates an initial compression over the Coanda surface with deleterious effects on ΔC_N. Note that the global normal force increments (at x/R=11.2) obtained for M_∞=0.7 and M_∞=0.9 is equivalent. This is noticeable since the control effect does not start at the same longitudinal position. At M_∞=0.7, a normal force increment is already induced at the nose cone/cylinder junction. At M_∞=0.9, it only starts downstream from the shock which is located at the boat-tail but it evolves quicker to reach the same integrated value as in the M_∞=0.7 case.

Use of Periodic and Continuous Blowing for the Spinning Projectile

Time-accurate unsteady simulations of the spinning configuration are presented in this section. Such computations have been performed to evaluate the Coanda jet efficiency in a configuration closer to the real-world application. The spin rate of the projectile is set to p=400 Hz. Control is performed on the spinning projectile using both continuous and pulsed jet.

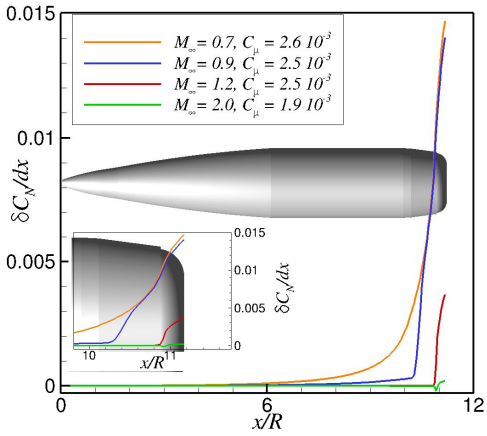

Figure 5. Streamwise integration of the normal force coefficient $\delta C_N/dx$ for the four Mach numbers at α=0°. Values of the momentum coefficient are almost identical.

COMPUTATIONAL DESCRIPTION

As shown in the previous section, no control capability has been demonstrated in supersonic flows. In the following section, the free stream Mach number is then restricted to M_∞=0.9. In order to limit the computational cost, only one incidence of α=3° is considered. Three different blowing configurations are used:

- a continuous jet. This configuration is denoted 1CJ-P400 (one continuous jet, p=400 Hz).
- one pulsed jet (1PJ-P400) operating at the spin rate of the projectile and which is activated on one-fourth of the spin cycle from -45° to +45° with 0° denoting the positive z-axis. This would permit to act always on the same sdirection.
- four pulsed jets (4PJ-P400) located every 90° along the circumference so that there is always one of them activated in the angular sector previously described.

Figure 6 presents the location of the four pulsed jets defined on the configuration 4PJ-P400. The angle φ denotes the time-dependent angular position of the red-colored jet situated on the positive y-axis at t/T=0. Concerning configuration 1PJ-P400 described above, only the red jet in figure 6 is used. Jet ducts are meshed for both subsonic and supersonic jets to ensure a more realistic velocity profile at the jet slot.

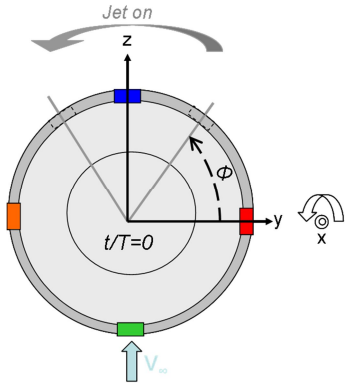

Figure 6. Locations of the four pulsed jets described in the configuration 4PJ-P400 at t/T=0. The grey angular sector indicates jets actuation area.

Note that the jet operating frequency is lower than the natural shedding frequency of the projectile (p=400 Hz to compare to $f=St_D \times U_\infty/D \approx 750$ Hz at $M_\infty=0.9$ and for $St_D=0.19$).

RESULTS

The temporal evolution of the normal force coefficient is outlined in figure 7 for a supersonic jet ($M_j=2.0$ and $pi_j=3.7$ bar) and for the three blowing configurations described above. Dashed lines designate spin averaged values for each case. Due to the axi-symmetric geometry, steady normal force coefficient is observed on the uncontrolled configuration. Using continuous blowing (1CJ-P400) leads to a sinusoidal evolution of C_N, with both positive and negative normal force increment. It can be noticed that the jet is at its maximum z-position at t/T=0.25 (φ=90°) but the normal force coefficient reaches its maximum value only at t/T=0.36 (φ=132°), where the jet is located at 42° from the z-axis. This issue will be discussed later. Moreover, the spin-averaged normal force coefficient for the configuration 1CJ-P400 is slightly lower than the one of the uncontrolled case. This can be explained by the fact that the local incidence of the flow with respect to the Coanda surface is less important at the lower side than at the upper side, improving the control performance. This was already observed by Rinehart et al. [7] on the Scorpion projectile, with the actuation located at the upper side of the projectile and negative angles of attack. The weak spin-averaged variation of C_N with respect to the uncontrolled case prevents the use of continuous blowing for effective control on a real-world application.

Concerning configuration 1PJ-P400, blowing is switched on at t/T=0.125 (φ=45°) and turned off at t/T=0.375 (φ=135°), with an active period corresponding to a physical time of 0.625 ms. As for the 1CJ-P400 configuration, the maximum normal force coefficient is obtained at t/T=0.36, which almost coincides to the jet shutdown. However, the pulsed jet actuation never reaches the same normal force level as the one of the 1CJ-P400 case. Note that an initial transient drop is marked at the beginning of the jet actuation (φ ranging from 45 to 48°). In the same way, an overload is observable after the jet shut-down (φ ranging from 135 to 137°). These two behaviors of the normal force coefficient were already noticed by Darabi and Wygnanski [10, 11] and are respectively due to positive pressures extending over the Coanda surface and to a dynamic stall vortex similar to the one seen over oscillating airfoils.

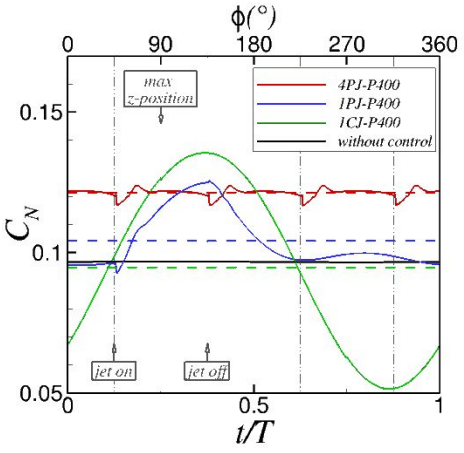

Figure 7. Time evolution of C_N for the uncontrolled case and the three controlled configurations at M=0.9 and α=3° (jet conditions are such that $M_j=2.0$ and $pi_j=3.7$ bar).

The more interesting configuration is clearly the 4PJ-P400 one. It allows a quasi-steady evolution of the normal force coefficient with a significant spin-averaged level of C_N with respect to the uncontrolled case.

Figure 8 displays instantaneous iso-contours of the pressure coefficient for the four cases described earlier. The jet is located at the upper side of the projectile for all cases. Free stream and jet conditions are identical. Furthermore, previous static results for the non-spinning projectile are added to allow the study of the rotation influence (denoted as the case 1CJ-P0). As emphasized by figure 8(b), the pressure coefficient C_p over the Coanda surface is affected by the projectile spin rate. Indeed, the low-pressure area due to the acceleration of the surrounding flow extends more azimuthally for the 1CJ-P400 case than for the 1CJ-P0 one. The differences in the pressure distribution between continuous and periodic actuation are highlighted comparing figure 8(b) and 8(c). The low-pressure area extends less in the 1PJ-P400 case than for the 1CJ-P400 one, which explains the weaker level of the normal force coefficient for periodic blowing on figure 7. Moreover, as shown by figure 8(c) and 8(d), there is a slight difference in the pressure distribution between the configuration using one pulsed jet (1PJ-P400) and the one using four pulsed jets (4PJ-P400). The influence of the latter jet actuation on the pressure distribution can be observed in figure 8(d), with a low-pressure area existing on the left of the jet location.

The azimuthal extension of the low-pressure area in the figure 8(b) can be explained considering the time taken by the jet to separate from the Coanda surface. To evaluate this time, we consider now the case without rotation 1CJ-P0. A controlled steady state using continuous actuation is used as initial flow condition. Then, the jet is shut down at t=0. The figure 9 illustrates the evolution of the normal force coefficient C_N and the evolution of the attached jet area S_{att}/S_c with respect to the dimensionless time $t^+=t\times U_\infty/L_{sep}$ after the jet shutdown. The length of the attached jet area L_{sep} is evaluated by $L_{sep}=R_c\times\theta_{sep}$, θ_{sep} denoting the maximum angle at which the jet detaches from the Coanda surface.

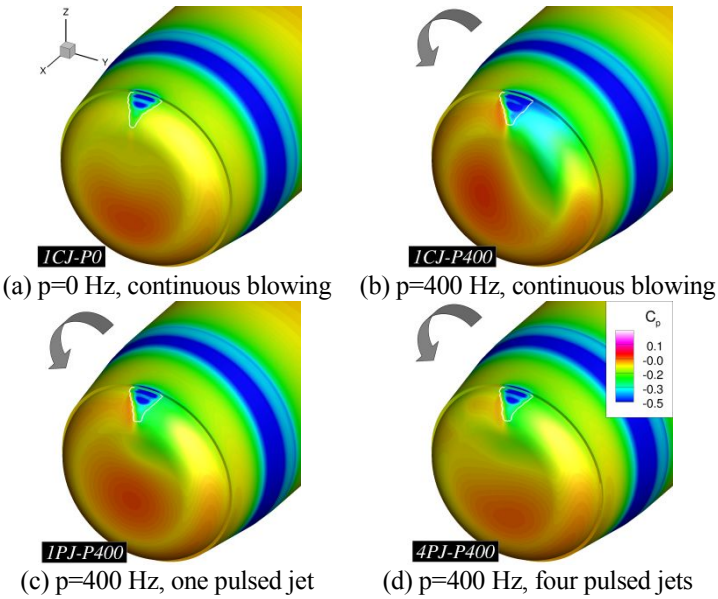

(a) p=0 Hz, continuous blowing (b) p=400 Hz, continuous blowing

(c) p=400 Hz, one pulsed jet (d) p=400 Hz, four pulsed jets

Figure 8. Colored iso-contours of the pressure coefficient C_p over the Coanda surface for both non-spinning and spinning projectiles. The jet is located at the upper side of the projectile. White lines indicate the jet separation location. Blowing conditions are such that M_j=2.0 and pi_j=3.7 bar.

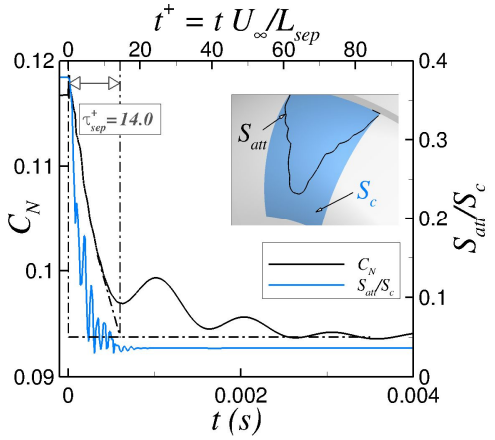

Figure 9. Evolution of C_N and S_{att}/S_c during a sequence of uncontrolled separation. The projectile spin rate is not taken into account and the initial flow is controlled with a continuous jet such that M_j=2.0 and pi_j=3.7 bar.

The characteristic dimensionless time τ_{sep}^+ indicates the duration to pass from the controlled value of C_N to the uncontrolled one. The definition of the attached jet area S_{att} and of the characteristic surface S_c is indicated in the top-right corner of figure 9.

As reported by Darabi and Wygnanski [11], this time does not depend on the initial controlled state (that is to say the value of C_μ). Shaqarin et al. [12] gathered several characteristic dimensionless times obtained for different control experiments. Authors highlighted that this parameter ranges from 14 to 25. In the present work, τ_{sep}^+ is approximately equal to 14. Considering now a rotation at a spin rate of p=400 Hz, this dimensionless time is equivalent to a rotation angle of 84°. This angle corresponds quite well to the azimuthal extension of the low-pressure area in the 1CJ-P400 case depicted in the figure 8(b). Moreover, this angle explains the phase difference between the instant where the jet is at its maximum z-position and the instant where C_N is maximum for continuous blowing (see curve for the 1CJ-P400 case in the figure 7). Indeed, the maximum value of C_N is obtained when this low-pressure area is centered around the z-axis which correspond to a phase difference of 84/2=42°, already noticed earlier.

CONCLUSIONS

This work described a computational attempt to control a 155 mm spin-stabilized projectile using Coanda effect. Current study focused on the feasibility of such a control concept on a large caliber projectile, for higher free stream Mach numbers. Simulations for spinning and non-spinning projectiles have been performed. Computations for the non-spinning projectile were achieved using continuous blowing. They revealed that the Coanda effect is not efficient for supersonic free stream Mach numbers. However, significant efforts are generated at M_∞=0.7 and 0.9. Evolutions of the normal force increment fit with the square root of the momentum coefficient at M_∞=0.7 and 0.9 using subsonic jets. This behavior corresponds to a circulation control. The momentum coefficient is the appropriate scaling parameter which permits to superimpose the normal lift increment for this two external Mach numbers.

More realistic spinning simulations were also achieved. The use of four pulsed jets acting in a 90° angular sector centered around the z-axis allows to obtain substantial spin-averaged normal force increment, almost identical to static simulations. Maximum normal force increments reached by the spinning projectile are more important than static ones, as a consequence of the larger extent of the low-pressure area induced by the control. The presence of this persistent low-pressure area is linked to the separation time of the jet.

This work highlighted the ability of Coanda effect to steer a 155 mm spin-stabilized projectile at high subsonic speeds. It has to be complemented with a system study to estimate requirements in terms of volume of compressed fluid (which will not necessary be air). A future study will also consider the use of synthetic jets to avoid pneumatic installations. Despite the synthetic jet velocity limitation, its large frequency range may be used to excite natural flow frequencies over the Coanda surface and improve the control efficiency.

ACKNOWLEDGMENTS

This study was partly funded by Nexter Munitions and by Onera - The French Aerospace Lab. It contributes to the research project "Manege" supported by the Ministry of Defence. The authors would like to acknowledge all members of the "DAAP-MHL" unit for their help on numerical issues. The authors thank as well all contributors to the research project "Manege".

REFERENCES

1. Patel, M., Sowle, Z., Ng, T.T. and Toledo, W. "Hingeless flight control of a smart projectile using miniature actuators," *AIAA Pape*r 2005-5258.
2. Massey, K., McMichael, J., Warnock, T. and Hay, F. "Mechanical actuators for guidance of a supersonic projectile," *Journal of Spacecraft and Rockets,* Vol. 45, No. 4, 2008.
3. Champigny, P. and Lacau, R. "Lateral jet control for tactical missiles," AGARD Special Course on Missile Aerodynamics, *ONERA*, 1994.
4. Riou, J. and Garnier, E. "Blowing effects on the separated flow over a moderately swept missile fin," *AIAA Journal,* Vol.49, No. 2, 2011, pp. 269-278.
5. McMichael, J., Lovas, A., Plostins, P., Sahu, J., Brown, G. and Glezer, A. "Microadaptive flow control applied to a spinning projectile," *AIAA Paper* 2004-2512.
6. Sahu, J. "Unsteady CFD modeling of aerodynamic flow control over a spinning body with synthetic jet," *AIAA Paper* 2004-747.
7. Rinehart, C., McMichael, J. and Glezer, A. "Transitory flow and force development on a body of revolution using synthetic jet actuation," *AIAA Paper* 2003-78.
8. Abramson, P., Rinehart, C., Vukasinovic, B. and Glezer, A. "Fluidic control of aerodynamic forces on a body of revolution," *AIAA Paper* 2007-4505.
9. Poisson-Quinton, P. and Lepage, L. "Survey of french research on the control of boundary layer and circulation," in *Boundary layer and flow control*, ed. By G.V. Lachmann, Vol. 1, Pergamon 1961.
10. Darabi, A. and Wygnanski, I. "Active management of naturally separated flow over a solid surface. Part 1. The forced reattachment process," *Journal of Fluid* Mechanics, Vol. 510, 2004, pp. 105-129.
11. Darabi, A. and Wygnanski, I. "Active management of naturally separated flow over a solid surface. Part 2. The separation process," *Journal of Fluid Mechanics* Vol. 510, 2004, pp. 131-144.
12. Shaqarin, T., Braud, C., Coudert, S. and Stanislas, M. "Open and closed-loop experiments to identify the separated flow dynamics of a thick turbulent boundary layer," *Experiments in Fluids*, Vol. 54, No. 2, 2013, pp. 1-22.